Materials Science Forum
ISSN: 1662-9752, Vol. 1185, pp 89-97
doi:10.4028/p-Fx9Ipm

Submitted: 2026-01-18
Revised: 2026-02-16
Accepted: 2026-02-24
Online: 2026-04-15

Tool Geometry Effect in Friction Stir Extrusion of Seamless Tubes from Aluminium Chips

Riccardo Puleo[1,a*], Salvatore Russo[1,b], Gianluca Buffa[1,c] and Livan Fratini[1,d]

[1]Department of Engineering, University of Palermo, Viale delle Scienze, Palermo 90128, Italy

[a*]riccardo.puleo01@unipa.it, [b]salvatore.russo18@unipa.it, [c]gianluca.buffa@unipa.it, [d]livan.fratini@unipa.it

Keywords: FSE, aluminium, recycling, extrusion, solid state.

Abstract. Nowadays, the growing demand for sustainable solutions in manufacturing has shifted research attention toward innovative recycling strategies. Among these, the Solid-State Recycling (SSR) technique has emerged as a viable approach to transform metal swarf into new products. Within the SSR family, friction stir extrusion (FSE) has gained particular interest as a promising method for producing wires from metal scraps, but recently, it was also employed for tube manufacturing. In literature, tube production via chip recycling often involves multi-step approaches, first consolidating/homogenizing the recycled chips and then extruding. In other cases, the tubes are manufactured directly from a bulk material, losing the sustainable goal. For this reason, this study aims to propose a single-step process in which aluminium chips are directly turned into a consolidated tube without any intermediate step. In addition, specific attention was given to the study of tool geometry, aiming to investigate the effect of a tapered tool's shape on the material flow and the overall process performance. Experimental tests were conducted to characterize the microstructure of extruded tubes and to calibrate numerical simulations employed for investigating process dynamics. Results revealed that the reduced contact diameter of the tapered tool generated lower processing temperatures but higher strain levels, fundamentally shifting the bonding mechanism from thermal assistance to mechanical dominance in oxide film breakage. Microstructural analysis demonstrated that the flat tool, characterized by predominant frictional heating and lower deformation, produced larger grain diameters due to thermally induced coarsening. Conversely, the tapered tool yielded significantly refined grain structures through severe plastic deformation and dynamic recrystallization under suppressed thermal conditions, indicating superior consolidation quality and enhanced particle bonding.

Introduction

The industrial sector accounts for approximately one quarter of global CO_2 emissions, reflecting the high energy intensity of large-scale material processing and transformation activities, with metals production representing a substantial contributor to this environmental burden due to its reliance on primary resource extraction and high-temperature processes [1]. Aluminum manufacturing, specifically, is responsible for roughly 3% of the world's direct industrial emissions [2]. As worldwide demand for aluminum continues to increase, driven by its favorable strength-to-weight ratio, corrosion resistance, and recyclability, which underpin extensive applications in the transportation, construction, and packaging sectors, the need to decouple resource consumption from economic growth has become increasingly critical to meet climate and sustainability targets [3]. Circular economy strategies provide a viable pathway to address this challenge by converting end-of-life products and manufacturing scrap into valuable secondary resources, thereby reducing dependence on energy-intensive primary production and limiting waste generation. Among circular economy approaches, recycling remains the dominant strategy for metallic materials due to their intrinsic ability to retain properties across multiple life cycles. Conventional aluminum recycling via remelting can reduce energy consumption by up to 90% relative to primary production, primarily because it eliminates the electrochemical reduction step and significantly lowers thermal energy requirements [4]. However, this route is affected by inherent inefficiencies, notably permanent material losses

arising from oxidation, dross formation, and alloy contamination during melting. These losses not only reduce material yield but also constrain the sustainability potential of conventional recycling, particularly for fine chips and low-quality scrap streams.

To address these limitations, solid-state recycling (SSR) techniques have emerged as innovative alternatives that completely bypass remelting, directly converting aluminum chips into semi-finished or finished products. SSR processes rely on the combined effects of temperature, pressure, and plastic deformation to achieve solid-state bonding between particles. The underlying mechanism involves the mechanical disruption of the stable oxide films naturally present on aluminum surfaces, enabling direct metal-to-metal contact and subsequent diffusion-driven bonding. Several SSR methodologies have been developed, each based on distinct mechanical principles to promote consolidation. Extrusion-based approaches, including direct hot extrusion and Equal Channel Angular Pressing (ECAP), impose severe plastic deformation that fragments oxide layers, enhances interparticle bonding, and refines the microstructure [5]. Friction-based methods, such as Friction Stir Extrusion (FSE) [6] and Friction Stir Consolidation (FSC) [7], exploit frictional heat generation and intense shear deformation to plasticize aluminum chips and weld them together under solid-state conditions. Sintering-based techniques, including Spark Plasma Sintering (SPS) and other field-assisted sintering methods, combine pulsed electrical currents, thermal energy, and compressive loads to promote diffusion bonding; however, they often require subsequent forming operations to achieve full densification due to limited strain introduction [8]. Among these approaches, direct extrusion processes represent a particularly promising SSR route, as they enable the transformation of loose chips into functional profiles, including hollow sections such as tubes, in a single continuous operation. The process mechanics involve feeding chips into a chamber where they undergo severe plastic deformation while being forced through an extrusion die, resulting in oxide dispersion, material densification, and effective solid-state bonding. The efficiency and quality of this transformation are strongly influenced by tool geometry, which governs material flow patterns, strain distribution, temperature evolution, and ultimately the resulting microstructural features and mechanical performance of the extruded product.

Tool design in extrusion processes has long been recognized as a critical factor affecting product quality in conventional manufacturing. However, its role in SSR processes, where the starting material consists of discrete particles with oxide-covered surfaces rather than continuous billets, introduces additional complexities. The tool geometry must not only guide material flow and shape the final profile but also ensure sufficient deformation to break oxide films and promote inter-particle bonding throughout the extruded section. Despite the importance of tool design in SSR extrusion, systematic investigations comparing different tool geometries and their effects on material consolidation and product quality remain limited in the literature.

The present study aims to elucidate the influence of tool geometry on the Friction Stir Extrusion (FSE) of seamless tubes produced from aluminum alloy chips, proposing a single-step manufacturing process able to convert chips directly into tubes. A comparative investigation is carried out on two distinct tool configurations: a conventional flat tool and a tool featuring a 20° chamfer at the shoulder-die interface. The flat geometry induces abrupt changes in material flow direction, whereas the tapered configuration promotes smoother material transition into the extrusion channel, altering local strain paths, pressure distribution, and flow continuity. The investigation integrates experimental campaigns with validated numerical simulations to provide a comprehensive assessment of both tool designs. Key process variables, including temperature distribution, strain accumulation, material flow patterns, and microstructural evolution, are analyzed to establish correlations between tool geometry and extruded tubes. Lastly, a microstructural analysis was carried out to enhance the effect of the different geometries. Understanding how these geometrical variations affect process mechanics, chip consolidation efficiency, and structural integrity of extruded tubes is essential for optimization and industrial scalability of SSR-based extrusion technologies.

Materials and Methods

Experimental campaign development.

A dry milling operation was carried out on an AA2024-O aluminum bar (62 HV) to produce machining chips, which were then cleaned in acetone for 30 minutes to ensure the best bonding performance and absence of contaminants. Successively, the chips were extruded using an ESAB LEGIO machine adapted for FSE (Figure 1a). A mass of 40 g of chips was loaded into a custom die chamber (76 mm in height and 25 mm in diameter), and two different tools were employed to consolidate the material into consolidated tubes (Figure 1b). Both tools had a nominal diameter of 23 mm; however, one featured a 20° taper, reducing the effective diameter to 22 mm (Figure 1c). Two experimental campaigns were conducted at a rotational speed of 1000 rpm and a vertical load of 15 kN to evaluate the effect of the tapered design on the material properties and process operating. Lastly, a K-type thermocouple was positioned at one-third of the die height, 1 mm from the inner die wall, to monitor temperature evolution during processing and to support calibration of the numerical simulations. Microstructural characterization was performed on longitudinal sections. Samples were mounted, ground, polished, and etched using Keller's reagent (2 mL HF, 3 mL HCl, 5 mL HNO_3, 190 mL H_2O). Observations were carried out with a GX51 Olympus optical microscope equipped with a 40× objective, and grain size was quantified using the mean linear intercept method (ASTM E112–96) in ImageJ.

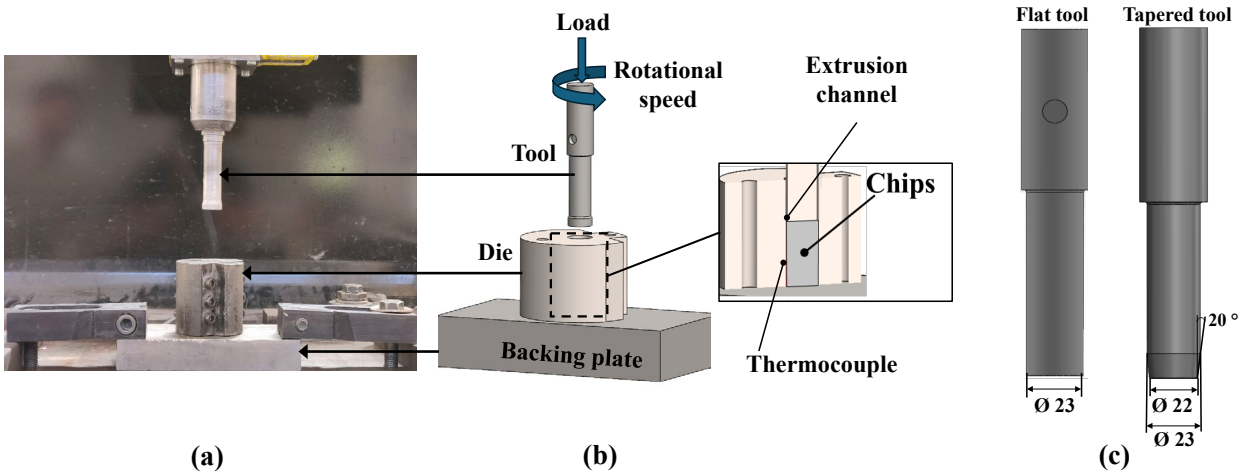

Fig. 1. (a) Experimental setup, (b) process components of the FSE technique, and (c) tools adopted for extruding tubes.

Numerical campaign modelling.

The numerical campaign was conducted in the SFTC DEFORM 3D environment (Figure 2a). The die, backing plate, and tools were modeled as H-13 rigid bodies with mesh sizes of 30000, 30000, and 60000 elements, respectively. A shear factor of 0.2 and interface heat transfer coefficients (IHTC) of 11, 45, and 45 W/mm²/K were assigned to model thermal exchange at the billet-tool, billet-die, and billet-backing plate interfaces. These values were determined through a coupled experimental-numerical temperature and torque calibration process (Figure 3), in which the simulated temperature and torque profiles were iteratively compared with the measured thermocouple data until an acceptable agreement was achieved. The corresponding thermal and shear parameters were then adopted for all simulations. This calibration step is essential to ensure a realistic representation of the process. During calibration, variations in the IHTC led to only minor changes in the predicted temperature fields, whereas variations of the friction parameters had a significantly greater influence on both temperature evolution and material response. Given the computational complexity associated with the explicit modelling of individual chips, the chip mass was represented as a single porous billet (Figure 2b) following the Shima-Oyane constitutive formulation [9]. This formulation is selectable in the Deform software, and it is based on a corrected Von Mises criterion that takes into account the

presence of microvoids in the material matrix (by implementing the relative density "R" in the formulation). The initial relative density of the porous material was experimentally determined considering the geometries of the system. Specifically, it was calculated as the ratio between the mass of chips loaded into the die chamber and the corresponding internal volume. The resulting relative density was set to 0.7, which represents the 70% of the density of the considered aluminium material. Lastly, to meet a compromise between computational time and quality of the results, the billet mesh consisted of 40000 elements, with a local refinement zone placed near the tool-material contact region (Figure 2b).

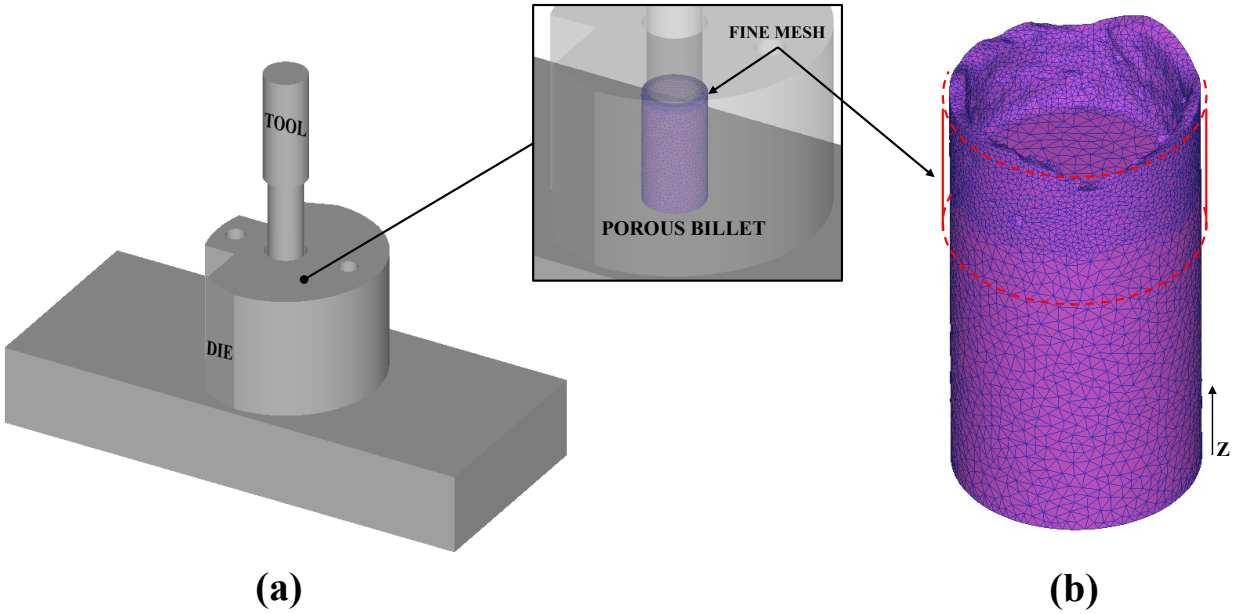

Fig. 2. (a) Numerical simulation modeling of the experimental FSE setup and (b) example of the mesh window for the early-extruded numerical tube.

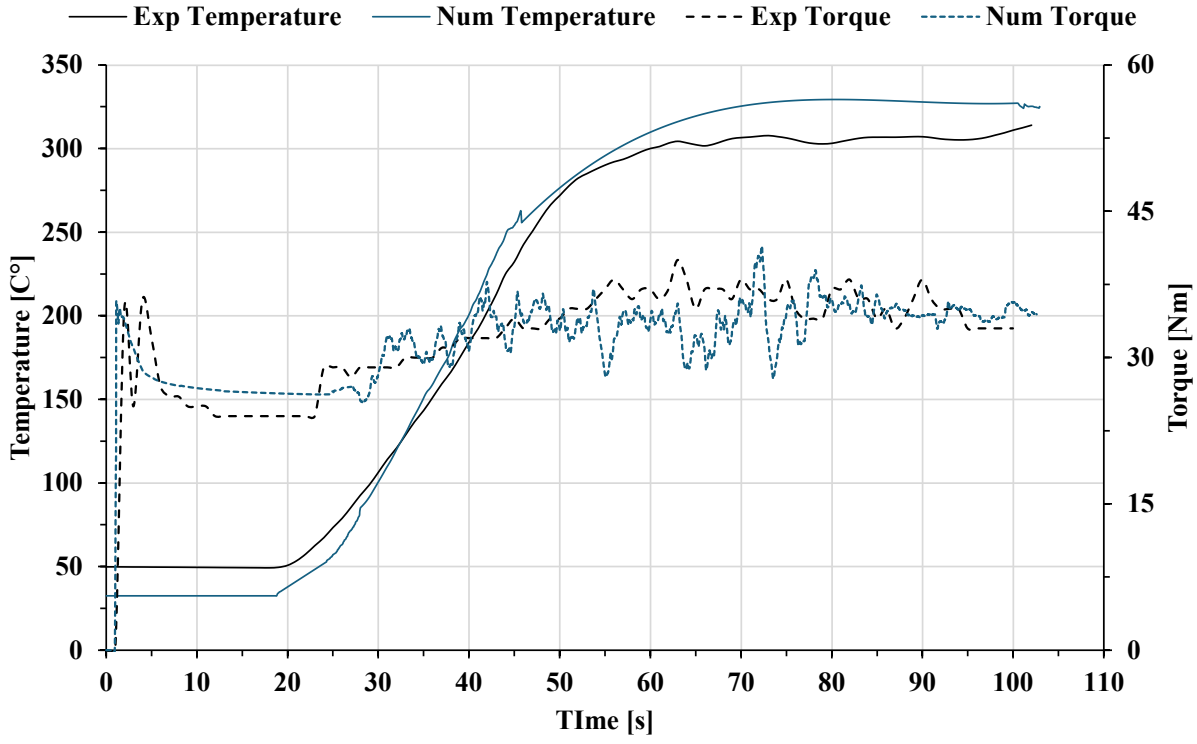

Fig. 3. Numerical calibration by means of experimental temperature and torque target profiles.

Results and Discussion

This section presents a comprehensive analysis of temperature evolution, strain accumulation, material displacement, and velocity field distributions. The numerical predictions are complemented by microstructural characterization of the tubes produced with both tool configurations, providing experimental validation and deeper insight into the correlation between process mechanics and material consolidation quality.

The numerical results obtained under steady-state conditions reveal significant differences in the thermo-mechanical behavior induced by the two tool geometries. As illustrated in Figure 4, the temperature and equivalent strain distributions along the longitudinal cross-sections of the extruded tubes demonstrate that the contact surface geometry significantly influences thermal generation. The reduced diameter of the tapered tool (Figure 4a) results in lower and more uniform frictional heating, yielding temperatures approximately 70 °C lower than those observed with the flat tool. Additionally, the larger contact area of the flat tool (Figure 4a) produces a distinct heat diffusion pattern in the vicinity of the tool-die clearance region (starting of the extrusion channel). Localized high-temperature zones are evident near the tool corners, which can be attributed to the severe material deformation imposed by the extrusion ratio and the associated flow restrictions within this region.

Strain distribution.

Regarding strain distribution (Figure 4b), both tool geometries generate substantial equivalent plastic strain throughout the extruded material, which is essential for oxide film fragmentation and inter-particle bonding. However, the flat tool induces higher strain concentrations near the tool-material interface and in the transition zone approaching the extrusion channel (in the range of 438-450). On the other hand, the tapered geometry promotes a more gradual strain accumulation, distributing deformation more uniformly across the material volume (in the range of 440-480). This difference in strain distribution patterns directly correlates with the material flow characteristics imposed by each tool configuration and has significant implications for consolidation quality and final tube properties.

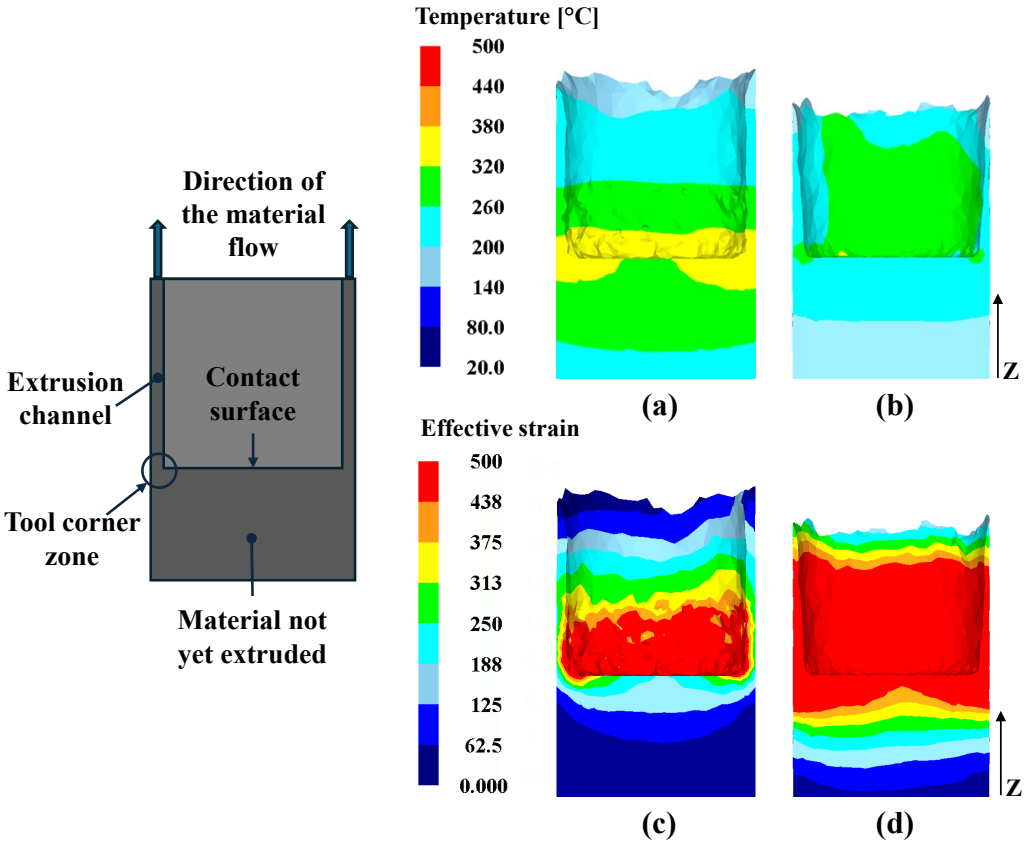

Fig. 4. (a) Temperature and (c) strain plot for the tube produced by the flat tool and (b) Temperature and (d) strain plot for the tube produced by the tapered tool.

Temperature distribution.

The temperature distribution results indicate that the larger contact surface area associated with the flat tool geometry generates greater heating. This thermal condition induces two competing mechanisms: material softening due to elevated temperature and resistance to material flow. The tapered tool enhances material flow through its inclined surface but generates higher strain than the flat configuration. This is due to its lower peak temperature (~300 °C) (Figure 4b), which reduces thermal softening and therefore requires greater plastic deformation to ensure proper consolidation (Figure 4d). Conversely, the elevated temperatures (~370 °C) generated by the flat tool enhance material softening, resulting in reduced strain accumulation during processing (Figure 4c). Furthermore, strain localization patterns differ significantly between the two geometries. The flat tool exhibits concentrated high-strain regions at the corners (~ 445), adjacent to the extrusion channel, whereas the tapered tool generates a more distributed zone of elevated strain in the corresponding area. This distinct deformation behavior directly reflects the influence of the local temperature field on material flow characteristics.

Displacement and velocity plots.

Material displacement and velocity fields along the extrusion direction (Z-direction) are presented in Figure 5, on the sectioned tube. The flat tool configuration (Figure 5a) induced significant flow obstruction, substantially affecting the displacement distribution in the tool vicinity. A wide region, extending several millimeters both above and below the tool, exhibited predominantly downward material displacement. This flow pattern indicates that the flat geometry redirected material away from the extrusion direction. In contrast, the tapered tool (Figure 5b) facilitated more streamlined material flow, resulting in visibly higher displacement along the extrusion direction and reduced downward-pushing effect. Moreover, the tube produced with the tapered tool exhibited a slightly shorter length compared to that obtained with the flat tool. This apparent contradiction can be justified by examining the strain distribution presented in Figure 4. Under the lower temperature conditions characteristic of the tapered tool configuration, greater plastic deformation is required to drive material through the extrusion die. At this point, the same volume of material undergoes more intensive straining, resulting in increased lateral flow and radial expansion rather than purely axial extension. This mechanism explains both the higher accumulated strain levels and the reduced final tube length observed in the tapered-tool case.

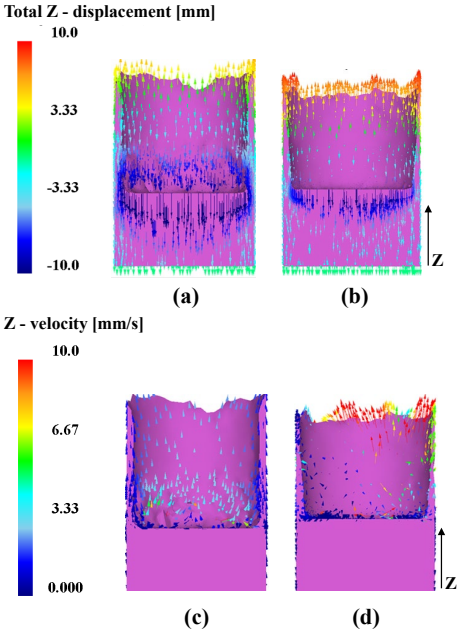

Fig. 5. Vector plots of the total (a) displacement and (b) velocity along the extrusion direction for the flat tool and vector plots of the total (b) displacement and (d) velocity for the tapered tool.

The enhanced displacement observed with the tapered tool is directly attributable to the velocity distribution. As shown in Figure 5d, the extrusion rate is markedly higher in the tapered configuration, with velocity vectors concentrated along the tube wall and exhibiting substantial magnitudes. Material is efficiently channeled through the extrusion die, promoting continuous flow with minimal hindrance. Conversely, the flat tool (Figure 5c) generates lower extrusion velocities due to its larger contact surface, which impedes material flow. The velocity distribution in this configuration appears more uniform across the tube wall, though with reduced overall magnitude, reflecting the restricted material displacement previously discussed.

Experimental results confirm this trend. Under the same process parameters, the tube length was 50 mm with the flat tool and 56 mm with the tapered tool. The usable length (without the unbonded chips at the top and the unextruded material at the bottom) was almost 30 mm and 35 mm, respectively. The average thickness was approximately 1 mm for both tubes, with minor variations attributable to eccentricity from manual tool–die alignment.

Microstructure analysis.

To assess the influence of tool geometry on microstructural evolution, transverse cross-sections were extracted from extruded tubes (Figure 6), and grain size measurements were performed close to the internal surface of the extruded tube. The analysis focused on regions experiencing distinct strain and temperature histories to elucidate the relationship between process variables and resulting microstructure.

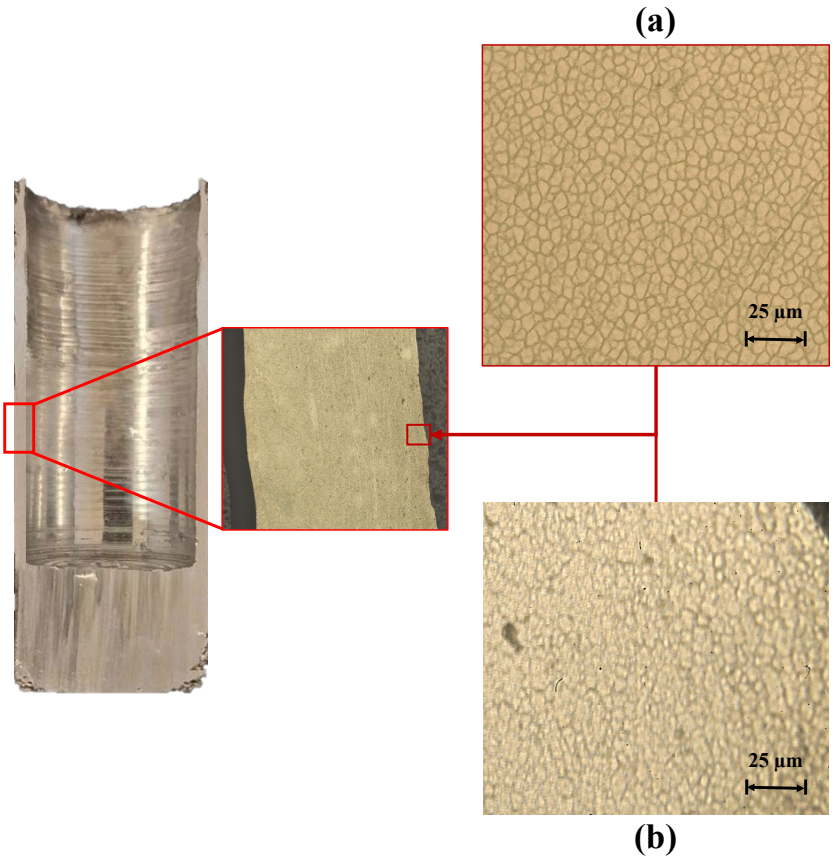

Fig. 6. Illustration of the longitudinal sections of the extruded tube, with the corresponding microstructural observations for the (a) tapered tool and (b) flat tool.

In the flat tool case (Figure 6b), characterized by higher processing temperatures and lower effective strain levels, frictional heating predominated as the primary heat source. Conversely, the reduced contact diameter of the tapered tool configuration (Figure 6a) minimized frictional heating. These distinct thermomechanical conditions directly influenced the observed microstructures. Material processed with the flat tool exhibited larger average grain diameters (avg. 4.3 ± 0.5 µm), attributable

to grain coarsening effects promoted by the elevated temperatures. The extended thermal exposure at higher temperature levels provided sufficient grain growth, partially offsetting any refinement achieved through plastic deformation. The lower strain accumulation in this configuration proved insufficient to counteract thermally induced coarsening, resulting in a relatively coarse final microstructure. In contrast, material extruded through the tapered tool displayed refined grain structure, with substantially smaller average grain diameters (avg. 4.1 ± 0.3 μm). The lower processing temperatures suppressed grain growth kinetics, while the intensified plastic deformation imposed severe shear strains that fragmented existing grains through dynamic recrystallization. The combination of reduced thermal coarsening and enhanced mechanical refinement resulted in a fine, equiaxed microstructure indicative of complete dynamic recrystallization.

Conclusion

In this paper, a single-step FSE process was successfully applied for producing consolidated tubes starting from aluminium chips. Two tools' geometries were tested through numerical simulations, along with a microstructural investigation. The following considerations were drawn:

- A single-step FSE process is capable of producing fully consolidated tubes.
- The numerical investigation revealed that the extended flat surface of the tool increases the frictional heat, promoting better material softening, but
- The material flow through the clearance between the tool and the die is hindered more for the flat tool than the tapered one. Despite the tapered tool offering fewer obstacles to flow, the reduced heat resulted in a higher strain level, demonstrating the predominance of a mechanical-drive process over the temperature-driven one that characterized the flat tool geometry.
- The reduced strain and high temperature combination, for the flat tool geometry, led to a visible grain coarsening compared to the tapered configuration, which limited the recrystallization phenomenon. A value of around 4.3 and 4.1 μm was observed for the flat and tapered tool, respectively.

Acknowledgment

This study was carried out within the MICS (Made in Italy – Circular and Sustainable) Extended Partnership and received funding from the European Union Next-Generation EU (PIANO NAZIONALE DI RIPRESA E RESILIENZA (PNRR) – MISSIONE 4 COMPONENTE 2, INVESTIMENTO 1.3 – D.D. 1551.11–10-2022, PE00000004). This manuscript reflects only the authors' views and opinions, neither the European Union nor the European Commission can be considered responsible for them.

References

[1] Bashmakov IA, Nilsson LJ, Acquaye A, Bataille C, Cullen JM, De La Rue Du Can S, et al., Contribution of Working Group III to the Sixth Assessment Report of the Intergovernmental Panel on Climate Change, (2022). https://doi.org/10.1017/9781009157926.013.

[2] Aluminium – IEA, information on https://www.iea.org/energy-system/industry/aluminium (accessed December 15, 2025).

[3] Watari T, Nansai K, Giurco D, Nakajima K, McLellan B, Helbig C., Global Metal Use Targets in Line with Climate Goals, Environ Sci Technol (2020) 54:12476–83. https://doi.org/10.1021/ACS.EST.0C02471.

[4] Ashby MF. The materials life cycle, Materials and the Environment (2021) 41–64. https://doi.org/10.1016/B978-0-12-821521-0.00003-7.

[5] Haase M, Ben Khalifa N, Tekkaya AE, Misiolek WZ. Improving mechanical properties of chip-based aluminum extrudates by integrated extrusion and equal channel angular pressing (iECAP), Materials Science and Engineering: A (2012) 539:194–204. https://doi.org/10.1016/J.MSEA.2012.01.081.

[6] Tang W, Reynolds AP. Production of wire via friction extrusion of aluminum alloy machining chips. J Mater Process Technol (2010) 210:2231–7. https://doi.org/10.1016/J.JMATPROTEC.2010.08.010.

[7] Li X, Baffari D, Reynolds AP. Friction stir consolidation of aluminum machining chips, The International Journal of Advanced Manufacturing Technology (2017) 94:5 2017;94:2031–42. https://doi.org/10.1007/S00170-017-1016-4.

[8] Paraskevas D, Dadbakhsh S, Vleugels J, Vanmeensel K, Dewulf W, Duflou JR. Solid state recycling of pure Mg and AZ31 Mg machining chips via spark plasma sintering, Mater Des (2016) 109:520–9. https://doi.org/10.1016/j.matdes.2016.07.082.

[9] Shima S, Oyane M. Plasticity theory for porous metals, Int J Mech Sci (1976) 18:285–91. https://doi.org/10.1016/0020-7403(76)90030-8.